Biosensors and Bioelectronics 123 (2019) 30–35

Contents lists available at ScienceDirect

Biosensors and Bioelectronics

journal homepage: www.elsevier.com/locate/bios

Development of an aptamer-based field effect transistor biosensor for quantitative detection of *Plasmodium falciparum* glutamate dehydrogenase in serum samples

Naveen K. Singh[a], Phurpa Dema Thungon[a], Pedro Estrela[b,*], Pranab Goswami[a,*]

[a] Department of Biosciences and Bioengineering, Indian Institute of Technology Guwahati, 781039 Assam, India
[b] Centre for Biosensors, Bioelectronics and Biodevices (C3Bio) and Department of Electronic and Electrical Engineering, University of Bath, Claverton Down, Bath BA2 7AY, United Kingdom

ARTICLE INFO

Keywords:
Aptamer
Field effect transistor
Plasmodium falciparum
Glutamate dehydrogenase
Malaria
Extended gate
Biosensor

ABSTRACT

There has been a continuous strive to develop portable, stable, sensitive and low cost detection system for malaria to meet the demand of effective screening actions in developing countries where the disease is most endemic. Herein, we report an aptamer-based field effect transistor (aptaFET) biosensor, developed by using an extended gate field effect transistor with inter-digitated gold microelectrodes (IDμE) for the detection of the malaria biomarker *Plasmodium falciparum* glutamate dehydrogenase (*Pf*GDH) in serum samples. A 90 mer long ssDNA aptamer (NG3) selective to *Pf*GDH was used in the aptaFET to capture the target protein. The intrinsic surface net charge of the captured protein led to change in gate potential of the aptaFET device, which could be correlated to the concentration of the protein. This biosensor exhibited a sensitive response in broad dynamic range of 100 fM −10 nM with limits of detection of 16.7 pM and 48.6 pM in spiked buffer and serum samples, respectively. The high selectivity of the biosensor for *Pf*GDH was verified by testing relevant analogous human and parasitic proteins on the device. Overall, the results validated the application potential of the developed aptaFET for diagnosis of both symptomatic and asymptomatic malaria.

1. Introduction

Malaria is a serious life threatening disease, affecting a large section of the population mostly in tropical and subtropical low and middle income countries (Gallup and Sachs, 2001; World Malaria Report, 2016). Usually, malaria is a curable disease if diagnosed and treated promptly and correctly. There are many reliable laboratory based methods available for malaria diagnosis. However, these methods are time-consuming, expensive and require skilled operators and hence, are not applicable for point of care diagnosis of malaria (Tangpukdee et al., 2009). Currently, lateral flow based immuno-chromatographic tests, commonly known as rapid diagnostic tests (RDTs), are widely used for detection of malaria. However, these antibody based RDTs are usually non-quantitative in nature and their stability is impaired in hot and humid environment (Ranadive et al., 2017). Over the last decade there has been a continuous strive to replace antibodies and other labile biorecognition elements with stable recognition systems for developing various diagnostic and detection devices (Thiviyanathan and Gorenstein, 2012). Among them, nucleic acid based aptamers are emerging as an efficient and viable alternative (Kakoti and Goswami, 2017). The binding affinity of ssDNA aptamers is usually comparable to antibodies. Aptamers can be produced economically in a large scale following established chemical protocols. Moreover, there is a scope for enhancing the selectivity of the DNA aptamers by chemical means (Song et al., 2012). There are few reports on developing aptamer-based malaria detection methods (Cheung et al., 2013; Jain et al., 2016; Singh et al., 2018a). These proof-of-concepts are mostly based on optical principles, while a few of them exploited electrochemical principles such as amperometry, voltammetry (Lee et al., 2012; Miranda et al., 2018) and impedance spectroscopy (Singh et al., 2018b; Chakma et al., 2018). However, each of these methods have their own merits and demerits as discussed in these reports. The focus of the current work is to explore a detection platform, amenable for integration into a portable device that complies well with the ASSURED (Affordable, Sensitive, Specific, User-friendly, Rapid and robust, Equipment free and Deliverable to end-users) mandate of WHO for application in developing and underdeveloped countries (Kunte and Kunwar, 2011).

The use of field effect transistor (FET) as a sensing platform has

* Corresponding authors.
E-mail addresses: p.estrela@bath.ac.uk (P. Estrela), pgoswami@iitg.ernet.in (P. Goswami).

https://doi.org/10.1016/j.bios.2018.09.085
Received 27 June 2018; Received in revised form 13 September 2018; Accepted 25 September 2018
Available online 26 September 2018
0956-5663/

gained enormous attention in diagnosis of various diseases (Estrela and Migliorato, 2007; Estrela et al., 2010; Formisano et al., 2016; Aliakbarinodehi et al., 2017). The major motivations for using FETs as biosensing platform are their high sensitivity, rapid response time, small size, and cheap fabrication process using integrated circuit technology. The FET system provides a sensitive and simple non-Faradic electrochemical measurement to monitor reactions occurring at the gate electrode surface, without using any redox marker (Park et al., 2012). In its simplest form, the FET measures variations in the open circuit potential that occur at the electrode interface. The extended gate FET (EgFET) was introduced to further increase the sensitivity and to overcome any instability issues that may occur during contact of FETs with biological liquids (Kaisti, 2017). In the EgFET structure, the gate of the transistor is extended away from the semiconductor and immersed in a solution for the measurement process, which gives an advantage to modify the surface of the extended gate chip as per the need of various sensing applications.

Malaria is caused by five different *Plasmodium* species amongst which, the *Plasmodium falciparum* is known to cause the most severe form of malaria (Robert et al., 2005). Many molecular biomarkers have been reported for the diagnosis of *P. falciparum* based malaria (Jain et al., 2014). The major motivation of using *P. falciparum* glutamate dehydrogenase (*Pf*GDH) as the target in the present investigation is its multifaceted advantages as a reliable biomarker and detection flexibility in the potentiometric transducer platform. Moreover, its human counterpart (HGDH) has not been reported in the matured human erythrocytes till date. The *Pf*GDH is structurally, kinetically, and sequentially (~77% amino acid) distinct from the host GDH (Wagner et al., 1998; Werner et al., 2005). This cytosolic *Pf*GDH with NADP-specific activity is present in the human serum with good detectable amounts during the infection (Acosta et al., 1998; Seol et al., 2017). The *Pf*GDH catalytic product of the reaction could be set in protonated form (α-ketoglutarate) using glutamate as the substrate which may furnish additional signal on the potentiometric platform once it is captured by the biorecognition element on the gate surface. Herein, we proposed an EgFET based detection of *P. falciparum* malaria using a selective aptamer as the biorecognition element against the biomarker, *Pf*GDH. The aptamer was immobilized via gold-thiol chemistry on inter digitated gold microelectrode (IDμE) connected to the gate of transistor (Scheme 1). A detailed account on the interesting findings is incorporated in this manuscript.

2. Experimental section

2.1. Materials

The ssDNA aptamer library and primers were obtained from IDT (USA). The selected thiolated NG3 aptamer (SH-(CH2)6-5′-TTT TCA CCT CAT ACG ACT CAC TAT AGC GGA TCC GAG CCG GGG TGT TCT GTT GGC GGG GGC GGT GGG CGG GCT GGC TCG AAC AAG CTT GC-3′ was synthesized by Sigma-Aldrich (UK). The Polyvinylidene fluoride (PVDF) was obtained from Amersham (UK), Syber gold (10,000×) was procured from Invitrogen (USA). The pGEMT easy TA cloning kit was received from Promega (USA). The starting blocking buffer containing a proprietary protein formulation in phosphate-buffered saline at pH 7.5 was obtained from Thermo Fisher (USA). The human serum from clotted male whole blood type AB was received from Sigma Aldrich. The proteins, *P. falciparum* lactate dehydrogenase (*Pf*LDH), *P. falciparum* Histidine rich protein-II (*Pf*HRP-II), *Pf*GDH and Human GDH (HGDH) were cloned, expressed and characterized in our lab previously (Jain et al., 2016; Chakma et al., 2016; Singh et al., 2018a). IDμE was procured from ASTAR, (Singapore). All other chemicals and reagents were of analytical grade and used as received. The compositions of all the buffers used in the current work are presented in Table S1, Supplementary Material.

2.2. Development and characterization of aptamer

SELEX (Systemic Evolution of Ligand by Exponential enrichment) was performed to produce specific ssDNA aptamers against *Pf*GDH as the target antigen from a random oligonucleotide library (10^{14}–10^{15}) as reported earlier (Singh et al., 2018a). The sequence were flanked with conserved primer binding sites (5′-CAC CTA ATA CGA CTC ACT ATA GCG GA-**N40**- GCA AGC TTG TTC GAG CCA G-3′) of which 40 mer sequence (**N40**) conferred the variation. Briefly, a total of 17 rounds of SELEX cycles were performed out of which 3 negative cycles against PVDF membrane and 2 negative cycles against control HGDH protein were executed to eliminate those aptamer candidates from the pool which have affinity for PVDF or HGDH. At the end of 17th cycle of SELEX, the amplified pool was cloned into pGEMT vector followed by transformation into *E. coli* DH5α competent cells. The positive clones were confirmed by restriction digestion and sequenced, aligned with Clustal X2 software for comparison. A dissociation constant (k_d) of 79.16 ± 1.58 nM for NG3 aptamer was discerned from surface plasmon resonance spectroscopy (Singh et al., 2018b). An electrophoretic mobility shift assay was performed to check the selectivity of the developed NG3 aptamer against *Pf*GDH (Fig. S1).

2.3. Determination of isoelectric point (pI) of PfGDH

The p*I* of the purified recombinant *Pf*GDH was measured by zeta potential study using a Zetasizer nano series (Malvern Instruments limited, U.K). The zeta potential of *Pf*GDH was measured in 50 mM appropriate buffers covering the pH values ranging from 2 to 10 in capillary cell (DTS1070- Malvern Instruments Limited) equipped with gold platted Beryllium/Copper electrode. A graph was plotted between the measured zeta potential values and the corresponding pH values. The p*I* of *Pf*GDH was identified from the pH scale at which the zeta potential becomes zero.

2.4. Electrode preparation and EgFET fabrication

An IDμE with dimension of 5 μm × 3200 μm for each fingers and 10 μm inter-spaces between the fingers was connected to a FET silicon oxide surface over an area of 0.8 cm × 1.6 cm following a reported design (Pui et al., 2013). The microelectrodes were UV-ozone cleaned for 30 min and then washed with streams of acetone, isopropanol and ethanol for 30 s each sequentially and followed by washing with ample amounts of mili-Q water (18.2 MΩ cm). The sample holding region with a holding capacity of 50 μl over the microelectrode was prepared by sealing the edges with molding tape. The fabrication of the biolayer over the cleaned gold electrode was performed by following a reported method (Jolly et al., 2016; Singh et al., 2018b). Briefly, 100 mM solution of 6 mercapto 1 hexanol (MCH) was prepared in absolute ethanol, which was further diluted to 1 mM in the binding buffer. The cleaned microelectrode surface was then incubated with 50 μl solution of thiolated aptamer: MCH in 1:100 ratio for 12 h in a humidity chamber. Prior to the immobilization over the electrode, the aptamer was treated at 90 °C for 5 min followed by cooling at 4 °C for 10 min to ensure that the aptamer is free from any hybridization. Following the immobilization procedure, the fabricated aptamer-IDμE was first cleaned with mili-Q water to remove unbound aptamer from the electrode surface and then it was further treated with 1 mM MCH for 1 h to ensure backfilling of any free spaces in the microelectrode. The electrode was further washed with mili-Q water and stem jet dry with nitrogen gas. Before analysis of samples, the aptamer/MCH gold microelectrode was treated with starting blocking buffer for 30 min to minimize the probability of non-specific interactions over the electrode surface.

The aptamers immobilized IDμE was connected to a home-designed n-type complementary metal oxide semiconductor (CMOS) field-effect transistor (MOSFET). The design, specification, and fabrication process of the MOSFET have been previously reported (Formisano et al., 2016)

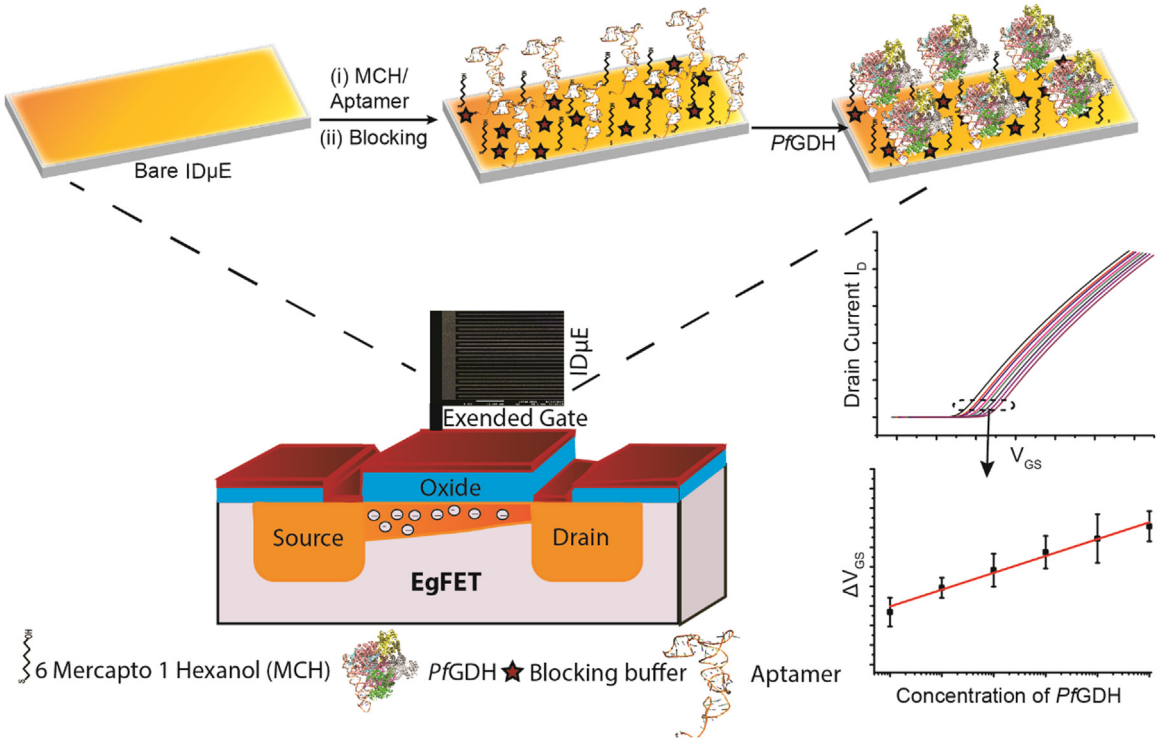

Scheme 1. Fabrication scheme of aptaFET for detection of *Pf*GDH in blood serum.

(EgFET circuit diagram in Fig. S2). In brief, single crystalline n-type MOSFETs were fabricated by using 0.7 μm CMOS technology with electrostatic discharge (ESD) protection circuits on the contact pads.

2.5. AptaFET measurement

The aptaFET measurement was performed by using a semiconductor device analyzer B1500A HR CMU (Agilent, USA). The EgFET was connected to an external IDμE and the measurement was performed over IDμE integrated with pseudo reference and working electrode. The FET transfer characteristics (drain current, I_D, vs. gate-to-source voltage, V_{GS}) were measured at a drain-to-source voltage (V_{DS}) of 50 mV varying the V_{GS} from 0 to 3 V. These settings protect the device from heating and reduce the risk of false measurements by the FET system. The aptamer-IDμE was incubated in FET measurement buffer until a stable signal was obtained. The electrode was then incubated in the binding buffer or diluted human serum (10 fold) spiked with different concentrations of *Pf*GDH protein for 30 min and washed with measurement buffer prior to the measurement. To ensure the interaction between aptamer and protein within the Debye length limitation, low ionic strength potassium phosphate buffer solution (PBS) or 10 fold diluted serum was used as measurement buffer (Chan et al., 1980; Stern et al., 2007). The Debye length κ^{-1} was calculated using Eq. (1) where ε_r is the relative permittivity, ε_o dielectric constant, k_B Boltzmann constant, T temperature, e elementary charge, N_A Avogadro number and I is the ionic strength of solution:

$$\kappa^{-1} = (\varepsilon_r \varepsilon_o k_B T / 2 N_A e^2 I)^{1/2} \quad (1)$$

All data presented here are the mean of at least three independent experiments performed with independent devices that are fabricated and investigated under similar conditions while the error bars represent the standard deviations. The statistical analysis was performed with Origin 8.0 software.

2.6. Atomic force microscopy (AFM) study

The topological characterization of the fabricated aptamer-IDμE was performed by AFM in continuous tapping mode using Multimode Nanoscope with IIIa controller (Bruker, Germany) in combination with control software (version 6). The AFM images were captured using 10 nm diameter AFM ContAl-G tips (Budget Sensors®, Bulgaria), and then analyzed with WsxM version 5 software.

2.7. Electrochemical impedance spectroscopy (EIS) study

The layer by layer fabrication of the aptasensor was characterized by means of Faradic EIS measurements in a three-electrode configuration with on-chip 2 mm gold as pseudo reference and counter electrodes. The measurements were performed in 10 mM PBS pH 8 with 10 mM ($K_3Fe(CN)_6/K_4Fe(CN)_6$) as redox probe using a μAutolab III/FRA2 potentiostat/galvanostat (Metrohm, The Netherlands) at equilibrium potential with 25 mV amplitude in the frequency range 100 kHz to 100 mHz. The Z- view software (Scribner associates) was used for curve fitting

3. Results and discussion

3.1. Characterization of aptamer-IDμE

AFM studies of the fabricated electrodes (Fig. 1A, B and Fig. S3D) revealed that the average height of the IDμE surface increased from ~1.35 ± 0.18 nm to ~1.48 ± 0.27 nm and ~1.71 ± 0.38 nm following immobilization of the aptamer/MCH layer and subsequent binding of the target protein, respectively. The surface root mean square roughness (R_{rms}) of the bare electrode increased from ~0.41 nm to ~0.53 nm following formation of the self-assembled monolayer (SAM) of aptamer/MCH which was however, reduced to ~0.47 nm after binding with the target protein. The surface topographical analysis of AFM images with peak distribution is shown in Fig. S3A-C. The surface modification was further characterized by EIS and obtained

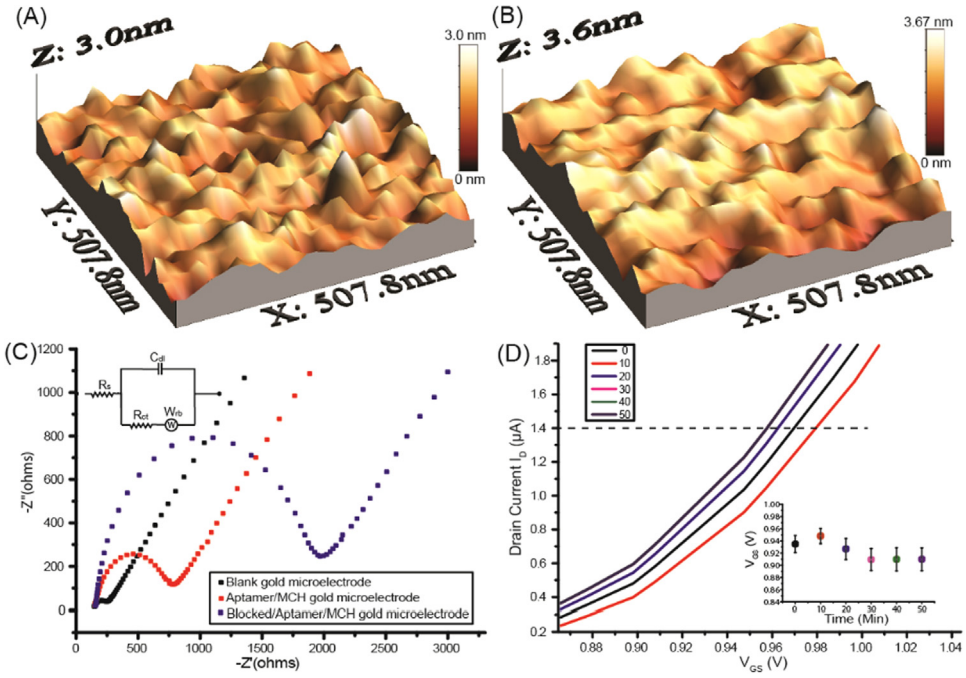

Fig. 1. AFM characterization of bare IDμE (A) and protein /aptamer- IDμE surfaces (B) (scanned area ~0.5 × 0.5 μm^2). (C) EIS characterization of blank and modified IDμEs. (D) AptaFET stability studies in binding buffer from the plot of drain current (I_D) versus gate voltage (V_{GS}) at different incubation time. Inset plot depicts gate voltage at fixed drain current verses different incubation time.

Nyquist plots were fitted with Randles- Ershler equivalent circuit model (inset of Fig. 1C) where R_s represents the solution resistance at higher frequency, C_{dl} the double layer capacitance formed at electrode-electrolyte interface, W is the Warburg impedance indicative as tail at lower frequency accounting for diffusion of charge from solution to electrode and R_{ct} the charge transfer resistance represented by the diameter of semicircle. Typical fitted values of these parameters for electrode modification are mention in Table S2. The R_{ct} value increased from ~118 ± 13 Ω for bare electrode to ~620 ± 47 Ω after co-immobilization of aptamer/ MCH and to ~1778 ± 68 Ω following subsequent treatment with MCH and starting blocking buffer. The reason for the increase in R_{ct} value following aptamer immobilization is attributed to the charge repulsion from the electrode surface caused by the negatively charged phosphate backbone of the DNA aptamer; further increase in R_{ct} value following the blocking step is ascribed to the accommodation of non-conducting protein in free areas of the gold electrode surface. The stepwise increase in impedance value confirmed the successful immobilization of the aptamer over the SAM layer on the IDμE surface.

3.2. Detection of PfGDH using aptaFET

Before starting the aptaFET detection of *Pf*GDH, the stability of the aptamer-IDμE was checked in FET measurement buffer by applying V_{GS} potentials from 0 to 3 V. A slight drift was observed, which was stabilized after 30 min of incubation (Fig. 1D). This change in response can be attributed to buried oxide site in surface assembled monolayer and which was reached to equilibrium by protonation/deprotonation of this oxide layer through the applied potential over time. The aptaFET measurement was performed at low ionic strength buffer to screen the probe-target interactions from the solution ions for gaining better sensitivity of the measurement as the presence of high counter ions in solution may shield the surface charge of the target protein. The negatively charged phosphate backbone of aptamer and the complementary positively charged amino acid moieties in protein induced complex formation between the target protein and the aptamer (Pethig and Kell, 1987). The net balanced charge produced on the electrode surface conferred by the target protein due to formation of the complex influenced the electric field in the FET. The developed surface charge could be detected within the electrical double layer (Goda and Miyahara, 2013), because the aptamer (NG3) – target (*Pf*GDH) interaction in the present case took place adjacent to the electrode surface due to smaller dimension of the aptamer. The relationship among the change in charge density (ΔQ), change in gate voltage (ΔV_{GS}), the number of bound proteins (N) having an effective electric charge per molecule (q), and the electric double layer capacitance (C_{dl}) effective within the Debye length may be projected as $\Delta V_{GS} = \Delta Q/C_{dl} = Nq/C_{dl}$ (Goda and Miyahara, 2012). Notably, the small size of the folded aptamer helps to overcome the Debye length limitation, which is normally exists with antibodies, thus provides freedom of using these DNA based recognition elements in FET measurements (Chu et al., 2017). The average distance of the aptamer from the electrode surface (average height of SAM layer - Average height of blank electrode) was calculated to be ~0.14 nm (Fig S3A, B). This proximal distance facilitated the biointeraction closer to electrode surface. A characteristic Debye length of ~1.5 nm was calculated from the Eq. (1) for FET measurement (Supplementary material). The aptamers known to undergo conformational change on their binding with the target molecules, and increase the charge density closer to electrode surface (Kakoti and Goswami, 2017; Aliakbarinodehi et al., 2017; Formisano et al., 2015). Thus, the interaction of the surface grafted aptamer with the target protein falls within the calculated Debye length limit. The *Pf*GDH is a globular protein. However, the spherical structure of the globular proteins is normally not sustained following their adsorption over the electrode surface because of the rearrangements through a multistep process. Here we assume that after adsorption over the electrode surface, the protein transformed into orthogonal shape (Goda and Miyahara, 2012) and the charge induced on the protein surface falls within the calculated Debye length facilitating the FET measurement as discuss below.

In the FET measurement, when the applied gate voltage (with respect to the source contact) is higher than the threshold voltage of the transistor, a conducting bridge is formed between drain and source. Under this condition when the voltage between drain and source become higher than zero ($V_{DS} > 0$), the flow of current through the channel under the influence of the electric field across the gate dielectric is initiated. In the operation of the EgFET, the change in magnitude of charge at the gate surface leads to a change in the threshold voltage, as seen by a shift on the drain current versus gate voltage (I_D *vs.* V_{GS}) (Chi et al., 2000). For the aptaFET measurement, the aptamer-IDμE was incubated with target *Pf*GDH protein spiked in diluted serum

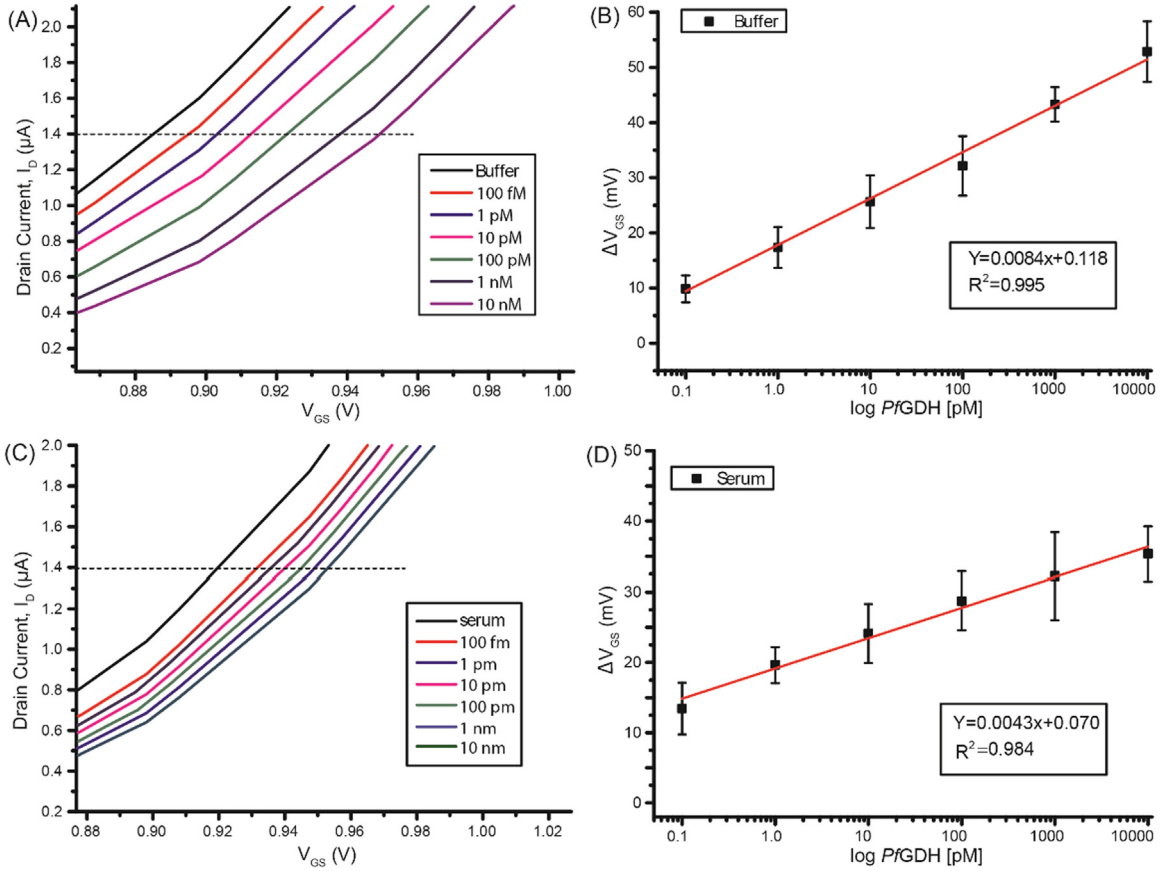

Fig. 2. AptaFET response against different concentrations of *Pf*GDH protein spiked in buffer (A) and serum (C) with corresponding calibration plots (B) and (D).

or binding buffer for 30 min. The response characteristics of the aptaFET are shown in Fig. 2, displaying incremental positive shifts of V_{GS} with the binding of *Pf*GDH protein in increasing concentrations, both in binding buffer (Fig. 2A) and in diluted serum (10 fold) (Fig. 2C) pH 8.0. This positive shift of gate voltage may be attributed to the increase in negative charge on the gate surface caused by the interaction of the negatively charged *Pf*GDH protein (p*I* of 6.6) with the folded aptamer within the Debye length as discussed above (for p*I* Fig. S4). This p*I* of *Pf*GDH was corroborated with the theoretically calculated isoelectric point (p*I* ~7.4) of *Pf*GDH (Wagner et al., 1998).

The calibration curves were generated by plotting varying concentrations of *Pf*GDH spiked in buffer and serum solutions against V_{GS} shift at a constant 1.4 μA drain current (Fig. 2B, D). A linear detection range of 100 fM to 10 nM for *Pf*GDH in both buffer and diluted serum was discerned. The aptaFET therefore offered *Pf*GDH detection towards much lower concentration range than the existing immune chromatographic dipstick method, which known to offers a detection range of 2–16 nM for malaria diagnosis (Li et al., 2005). The limits of *Pf*GDH detection (LOD = 3 × SD of blank/ slope of calibration curve) discerned from the corresponding calibration plots were 16.7 pM and 48.6 pM in buffer and diluted serum, respectively. The sensitivities of the aptaFET sensor were calculated from the calibration plots (Fig. 2B, D) and found to be 8.40×10^{-6} V/log ([*Pf*GDH] pM) (R^2 = 0.99) in buffer solution and 4.30×10^{-6} V/ log ([*Pf*GDH] pM) (R^2 = 0.98) in diluted serum. A minor reduction in sensitivity and increase in LOD value in serum medium have been attributed to the complex nature of the chemical environment in serum samples causing hindrance to aptamer-*Pf*GDH interaction. Moreover, the presence of extra solvated ions in serum is affecting the Debye screening length and hence, lowering the effective charge of the biomolecules. The minor reduction of these performances however, may not have much effect on the diagnosis of malaria considering the serum concentration level of this biomarker under the diseased conditions (Li et al., 2005). The selectivity of the developed aptaFET biosensor analyzed in 10 nM each of the analogous human proteins (HGDH, HSA) and malaria proteins (*Pf*LDH, *Pf*HRP-II) spiked in buffer, showed much weaker signal (ΔV_{GS}) as compared to the target (*Pf*GDH) protein (Fig. 3A, B). The results validated high selectivity of the developed aptaFET biosensor suitable for analysis of real sample for malaria diagnosis.

4. Conclusions

Herein, a novel aptaFET biosensor for selective detection of *P. falciparum* specific biomarker *Pf*GDH in serum sample has been reported. The device utilized an interdigitated gold micro electrode connected with extended gate of transistor offering easy immobilization of the DNA-aptamer over it and sensitive detection of the target biomarker in solution without impairing the FET functions. The aptaFET biosensor offered response time in seconds (~5 s), detection limit down to pico molar level (48.6 pM), and detection range in lower concentration region (0.1 pM to 10,000 pM) in diluted serum samples. This detection capability of the aptaFET biosensor would be suitable for its application in diagnosis of symptomatic as well as asymptomatic malaria including the analysis of parasitemia level during regression of parasitic load under medication. Notably, the minimum *Pf*GDH concentration in serum of malaria patients including in asymptomatic malaria, usually lies in nanomolar range (Li et al., 2005). We compared the response of the aptaFET with other reported portable biosensors (Table S3), and found that the presented biosensor exhibited superior detection range under lower concentration region, lower response time and comparable LOD values for *Pf*GDH (Markwalter et al., 2016; Chakma et al., 2016; Lillehoj et al., 2013; Dirkzwager et al., 2016; Newman et al., 2008; Jimenez et al., 2017). This FET-based potentiometric sensor offered reliable results with the sufficiently diluted serum samples that

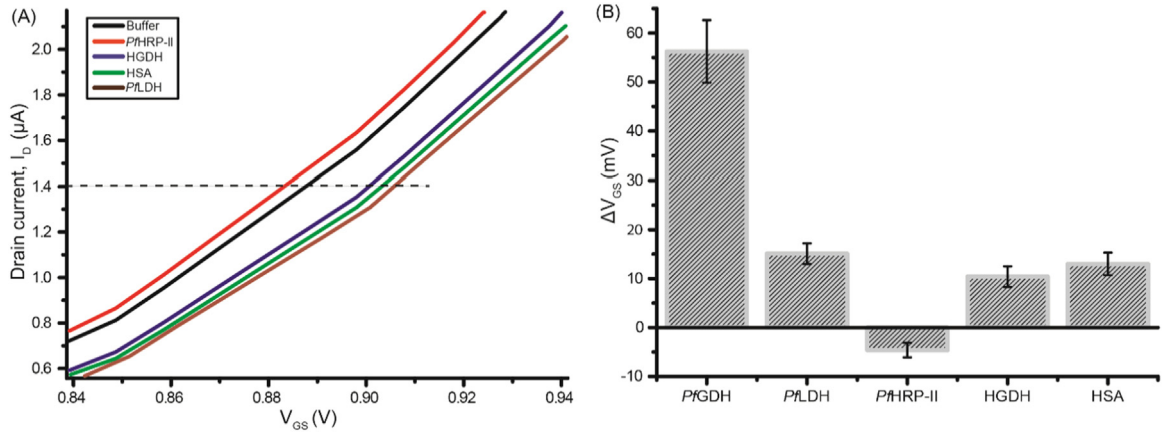

Fig. 3. (A) AptaFET response against different potential interfering proteins. The analysis was performed in FET measurement buffer with 30 min of incubation time; shift in gate voltage (V_{GS}) was monitored at 1.4 μA drain current (I_D). (B) Selectivity of the aptaFET biosensor for analogous proteins. Mean data with standard deviations from triplicate experiments are presented.

minimized the screening effect of the sample ions on the gate potential. We validated the function of the device well ≤10 mM of the sample salts, which may be attained by diluting the serum by ~10 folds. This miniaturized aptaFET with extended IDμE delivered label free detection capability through direct readout of the intrinsic net charge of the capture target molecule (*Pf*GDH) making the measurement easy and swift. Further integration of the developed device with a portable electrochemical system for data measurement will make this aptaFET suitable for implementing in POC settings.

Acknowledgements

We acknowledge financial assistance from British Council Newton-Bhabha Fund: PhD Placement grant (Grant no. BT/IN/UK/DBT-BC/16–17). We also acknowledge Department of Biotechnology, Government of India for Grant No. BT/PR13560/ COE/34/44/2015 Project II.

Appendix A. Supporting information

Supplementary data associated with this article can be found in the online version at doi:10.1016/j.bios.2018.09.085.

References

Aliakbarinodehi, N., Jolly, P., Bhalla, N., Miodek, A., De Micheli, G., Estrela, P., Carrara, S., 2017. Sci. Rep. 7, 44409.
Acosta, A.R., Domínguez, N.G., Aguilar, I., Girón, M.E., 1998. Braz. J. Med. Biol. Res. 31 (9), 1149–1155.
Chan, D.C., Pashley, R.M., White, L.R., 1980. J. Colloid Interface Sci. 77 (1), 283–285.
Chakma, B., Jain, P., Singh, N.K., Goswami, P., 2016. Anal. Chem. 88 (20), 10316–10321.
Chakma, B., Jain, P., Singh, N.K., Goswami, P., 2018. Electroanal 30, 1839–1846.
Cheung, Y.W., Kwok, J., Law, A.W., Watt, R.M., Kotak, M., Tanner, J.A., 2013. PNAS 110 (40), 15967–15972.
Chi, L.L., Chou, J.C., Chung, W.Y., Sun, T.P., Hsiung, S.K., 2000. Mater. Chem. Phys. 63, 19–23.
Chu, C.H., Sarangadharan, I., Regmi, A., Chen, Y.W., Hsu, C.P., Chang, W.H., Lee, G.Y., Chyi, J.I., Chen, C.C., Shiesh, S.C., Lee, G.B., Wang, Y.L., 2017. Sci. Rep. 7, 5256.
Dirkzwager, R.M., Liang, S., Tanner, J.A., 2016. ACS Sens. 1 (4), 420–426.
Estrela, P., Migliorato, P., 2007. Mater. Chem. 17, 219–224.
Estrela, P., Paul, D., Song, Q., Stadler, L.K.J., Wang, L., Huq, E., Davis, J.J., Ko Ferrigno, P., Migliorato, P., 2010. Anal. Chem. 82, 3531–3536.
Formisano, N., Bhalla, N., Heeran, M., Reyes Martinez, J., Sarkar, A., Laabei, M., Jolly, P., Bowen, C.R., Taylor, J.T., Flitsch, S., Estrela, P., 2016. Biosens. Bioelectron. 85, 103–109.
Formisano, N., Jolly, P., Bhalla, N., Cromhout, M., Flanagan, S.P., Fogel, R., Limson, J.L., Estrela, P., 2015. Sen. Actu. B Chem. 220, 369–375.
Gallup, J.K., Sachs, J.D., 2001. Am. J. Trop. Med. Hyg. 64 (12), 85–96.
Goda, T., Miyahara, Y., 2012. Lang 28 (41), 14730–14738.
Goda, T., Miyahara, Y., 2013. Biosen. Bioelectr. 45, 89–94.
Jain, P., Chakma, B., Singh, N.K., Patra, S., Goswami, P., 2016. Mol. Biotechnol. 58.
Jain, P., Chakma, B., Patra, S., Goswami, P., 2014. Biomed. Res. Int (2014/852645).
Jimenez, A., Channer, R., Perera, R., Gamboa, D., Chiodini, P.L., González, I.J., Mayor, A., Ding, X.C., 2017. Malar. J. 16, 128.
Jolly, P., Tamboli, V., Harniman, R.L., Estrela, P., Allender, C.J., Bowen, J.L., 2016. Biosens. Bioelectron. 75, 188–195.
Kakoti, A., Goswami, P., 2017. BBA General. Subj. 1861, 3289–3299.
Kaisti, M., 2017. Biosens. Bioelectron. 98, 437–448.
Kunte, R., Kunwar, R., 2011. MJAFI 67 (4), 376.
Lee, S., Song, K.M., Jeon, W., Jo, H., Shim, Y.B., Ban, C., 2012. Biosens. Bioelectron. 35, 291–296.
Li, Y., Ning, Y.S., Li, L., Peng, D.O., Dong, W.Q., Li, M., 2005. Di Yi Jun Yi Da Xue Xue Bao 25 (4), 435–438.
Lillehoj, P.B., Huang, M.C., Truongc, N., Hod, C.M., 2013. Lab Chip 13 (2950-295).
Markwalter, C.F., Davis, K.M., Wright, D.W., 2016. Anal. Biochem. 493, 30–34.
Miranda, G.F., Feng, L., Shiu, S.C., Dirkzwager, R.M., Cheung, Y.W., Tanner, J.A., Schöning, M.J., Offenhäusser, A., Mayer, D., 2018. Sens. Actuators B Chem. 255, 235–243.
Newman, D.M., Heptinstall, J., Matelon, R.J., Savage, L., Wears, M.L., Beddow, J., Cox, M., Henk, D.S., Mens, P.F., 2008. Biophys. J. 95 (2), 994–1000.
Park, S.J., Kwon, O.S., Lee, S.H., Song, H.S., Park, T.H., Jang, J., 2012. Nano Lett. 12, 5082–5090.
Pui, T.S., Kongsuphol, P., Arya, S.K., Bansal, T., 2013. Sens. Actuators B: Chem. 181, 494–500.
Pethig, R., Kell, D., 1987. Phys. Med. Biol. 32, 933.
Ranadive, N., Kunene, S., Darteh, S., Ntshalintshali, N., Nhlabathi, N., Dlamini, N., Chitundu, S., Saini, M., Murphy, M., Soble, A., Schwartz, A., Greenhouse, B., Hsiang, M.S., 2017. Clin. Infect. Dis. 64, 1221–1227.
Robert, W.S., Carlos, A.G., Abdisalan, M.N., Hla, Y.M., Simon, I.H., 2005. Nature 434, 214–215.
Seol, B., Shin, H.I., Kim, J.Y., Jeon, B.Y., Kang, Y.J., Pak, J.H., Kim, T.S., Lee, H.W., 2017. Malar. J. 16, 3.
Singh, N.K., Chakma, B., Jain, P., Goswami, P., 2018a. ACS Comb. Sci. 20 (6), 350–357.
Singh, N.K., Arya, S.K., Estrela, P., Goswami, P., 2018b. Biosens. Bioelectron. 117, 246–252.
Stern, E., Wagner, R., Sigworth, F.J., Breaker, R., Fahmy, T.M., Reed, M.A., 2007. Nano Lett. 7 (11), 3405–3409.
Song, K.M., Lee, S., Ban, C., 2012. Sensors 12, 612–631.
Thiviyanathan, V., Gorenstein, D.G., 2012. Proteom. Clin. Appl. 6 (0), 563–573.
Tangpukdee, N., Duangdee, C., Wilairatana, P., Krudsood, S., 2009. Korean J. Parasitol. 47 (2), 93–102.
Wagner, J.T., Lüdemann, H., Färber, P.M., Lottspeich, F., Krauth, S.R.L., 1998. Eur. J. Biochem. 258, 813–819.
Werner, C., Stubbs, M.T., Krauth, S.R.L., Klebe, G., 2005. J. Mol. Biol. 349, 597–607.
World Health Organization, 2016. World Malaria Report 2016. World Health Organization, Geneva. 〈http://www.who.int/malaria/publications/world-malaria-report-2016/report/en/〉.